Sub-step Methodology for Coupled Monte Carlo Depletion and Thermal Hydraulic Codes

D. Kotlyar and E. Shwageraus

Department of Engineering, University of Cambridge
CB2 1PZ, Cambridge, United Kingdom

Keywords:
Monte Carlo; depletion; thermal-hydraulics; coupling; sub-step; BGCore

Abstract

The governing procedure in coupled Monte Carlo (MC) codes relies on discretization of the simulation time into time steps. Typically, the MC transport solution at discrete points will generate reaction rates, which in most codes are assumed to be constant within the time step. This assumption can trigger numerical instabilities or result in a loss of accuracy, which, in turn, would require reducing the time steps size. This paper focuses on reducing the time discretization error without requiring additional MC transport solutions and hence with no major computational overhead. The sub-step method presented here accounts for the reaction rate variation due to the variation in nuclide densities and thermal hydraulic (TH) conditions. This is achieved by performing additional depletion and TH calculations within the analyzed time step. The method was implemented in BGCore code and subsequently used to analyze a series of test cases. The results indicate that computational speedup of up to a factor of 10 may be achieved over the existing coupling schemes.

1. Introduction

Many Monte Carlo (MC) coupled computer codes have been developed and are widely used to perform reactor designs and fuel cycle analyses (Bomboni et al., 2010). Coupled codes, such as SERPENT (Leppänen et al., 2015), BGCore (Fridman et al., 2008) and MCNPX (Fensin et al., 2010) are just a small subset of such codes, in which the MC transport solution is linked to a deterministic point depletion solver. There is an ongoing effort to expand the use of such MC based codes to full core analysis (Leppänen et al., 2014). Therefore, there is a need to introduce additional feedback that will account for variation in thermal-hydraulic (TH) conditions in the coupled calculation routine.

The coupling schemes implemented by the various codes typically rely on explicit methods to couple between MC transport solution and burnup with TH calculations. The explicit nature of these coupling schemes relates to the time integration. Recently however, a major deficiency in such explicit coupling methods was reported (Dufek et al., 2013a and Kotlyar and Shwageraus, 2013). Non-physical behavior of the results in a form of oscillations in various local parameters, such as the neutron flux distribution was observed and studied. The mentioned studies showed that large systems (e.g. 3D fuel assemblies or cores) may exhibit such unphysical behavior. Previous results also indicated that the trigger for such numerical instabilities could relate, for example, to slightly asymmetrical flux distribution which may be caused by poor spatial convergence of MC statistics. However, the asymmetry in flux distribution could also be due to an asymmetric distribution of burnup or TH parameters such as coolant density, which is often the case in realistic core conditions. These studies concluded that the issues were linked to the use of explicit coupling methods during time integration. In other words, reducing the length of the time-step to sufficiently small value would be required to eliminate the instability issues.

Therefore, new coupling methods have been developed first for MC-burnup applications (Dufek et al., 2013b) and implemented in Serpent and BGCore. Then, more comprehensive fully coupled MC-burnup-TH schemes (Kotlyar and Shwageraus, 2014) were proposed and implemented in BGCore. The stability issues were resolved through the use of alternative methods such as the Stochastic-Implicit-Euler (SIE) and Stochastic-Implicit-Mid-point (SIMP) methods. The methods solve

the depletion and TH problems simultaneously and iteratively. Each iteration updates either the end-of-step (SIE) or middle-of-step (SIMP) flux, which is weighted with variable under-relaxation factor and combined with the values obtained in previous iterations.

Recent studies (Kotlyar and Shwageraus, 2016) indicated that the efficiency of the SIE may be quite poor. More specifically, in order to obtain accurate results, the time discretization steps are required to be extremely small, which increases the overall calculation time. Although, the same study indicated that the SIMP method considerably improves the accuracy of the results, the computational efficiency is still relatively low. The SIE method, for example, relies on the end-of-step (EOS) reaction rates to calculate the EOS nuclide densities, similarly to the explicit methods that rely on the beginning-of-step (BOS) reaction rates. The reason for superior performance of the SIMP method is that the middle-of-step (MOS) reaction rates are assumed to be timestep representative, which is certainly a better approximation than using fixed BOS or EOS reaction rates. However, none of these assumptions are suitable for many practical problems with rapid change of neutron energy spectrum such as Gadolinium depletion.

One of the options to improve the original SIE methods was to include a sub-step approach. Previous studies (Kotlyar and Shwageraus, 2016) introduced the sub-step methodology for coupled MC depletion solution and fixed TH conditions. The method was implemented in BGCore and used a log-linear correlation between the nuclide densities and reaction rates to better account for the variation in reaction rates within the time step. The method required only additional depletion calculations to be carried out but no additional transport calculations. This method was implemented in BGCore code, which was subsequently used to analyze a number of test cases for a typical PWR fuel assembly. The results systematically showed that the method outperforms the original SIE and SIMP methods in accuracy and computational efficiency.

The current research seeks to extend the previously proposed sub-step method by accounting for the variation in TH properties within the analyzed time step. The variation in TH conditions will in turn lead to variation in reaction rates as well. Therefore, the first stage of this research was to develop reasonably accurate correlations between the reaction rates and nuclide densities as well as TH conditions. These correlations that link fuel temperatures (or any other TH conditions) and

nuclide densities are constructed on the fly. Each iteration within the analyzed timestep adds an extra data point, from which the reaction rates calculated from the MC transport are linked to a unique fuel temperature and nuclide density set. The sub-step sequence within each time step starts at BOS, for which the reaction rates are known. Depletion with BOS reaction rates allows to obtain the end of sub-step nuclide densities. Then, the new reaction rates are updated from the constructed correlations by substituting the updated nuclide densities. These updated reaction rates are used to calculate the new TH conditions, which are then used to update the reaction rates according to the correlations. This procedure is subsequently performed for the following sub-steps within the calculated time step. This is a coupled routine since reaction rates are continuously updated, however the scheme requires no additional MC solutions. This method was implemented in BGCore and was used to perform various 3D test cases. The results indicate that this method allows to achieve accurate results with considerably larger time steps than required with other coupling methods considered and compared in this study (e.g. explicit, SIE and SIMP).

2. BGCore description

The proposed coupled sub-step method was programmed into BGCore system. BGCore is a system of codes in which Monte-Carlo code MCNP4C (Briesmeister et al., 2000) is coupled with fuel depletion and thermal-hydraulic (TH) modules. BGCore utilizes multi-group methodology for calculation of one-group transmutation cross-sections (Haeck et al., 2007; Fridman et al., 2008) which significantly improves the speed of burnup calculations. In addition to the depletion module, BGCore system also includes a built-in thermal-hydraulic (TH) feedbacks module. The modules are executed iteratively so that the coupled system is capable of predicting fuel composition, power, coolant density and temperature distributions in various types of reactor systems (Kotlyar et al., 2011).

3. Burnup-thermal hydraulic coupling methodology

Coupled burnup-TH analyses are used to account for the strong relation between the various neutronic and thermal hydraulic parameters. The nuclide densities, **N**, and TH properties, **T**, depend on each other and also on the energy and space distribution of neutron flux, ϕ. However, calculation of ϕ requires a prior knowledge of **N** and **T**. Practicality, the solution of such time-dependent non-linear problem is obtained by discretizing the simulated time period into time steps. Within a time step, the parameters of interest, such as nuclide densities are computed by assuming that other parameters, such as reaction rates remain constant during the time step. Generally, this assumption may lead to a loss of accuracy when the time steps are not sufficiently small.

The non-linear problem mentioned above can be described by three coupled equations. The first is the neutron transport eigenvalue equation that provides reaction rates, denoted here as $\boldsymbol{\mathcal{M}}$. In this work, the neutron transport operator will be denoted by φ. The MCNP4C code is used here to obtain the reaction rates $\boldsymbol{\mathcal{M}} = \varphi(\mathbf{N}, \mathbf{T})$ for a known mixture of nuclides **N** and TH conditions **T**. The second is the heat balance equation that computes the temperature distribution from which also the coolant and/or moderator densities can be derived. The operator for solving the heat conduction and convection problem, which requires the reaction rates as an input, is denoted here as $\Upsilon(\boldsymbol{\mathcal{M}})$. The last is the burnup equation that determines the change in nuclide densities during time *t*, as described in Eq. 1.

In order to progress in time, a set of first order Bateman equations (Bateman, 1932) have to be solved. This solution is known as matrix exponential (Eq. 1).

$$\mathbf{N}(t) = e^{\boldsymbol{\mathcal{M}}\Delta t}\mathbf{N}(0) \tag{1}$$

where, $\mathbf{N} = [n_1 \cdots n_n]$ is unique for a certain time point and n_j is the atomic density of nuclide *j*. The operator $\boldsymbol{\mathcal{M}}$ in Eq.1 represents the transmutation matrix that includes removal terms on its diagonal and production rates on the off-diagonal locations as explained in Eq.2:

$$\begin{aligned} M_{j,j} &= -\lambda_j - \sigma_j\phi \\ M_{j,k\neq j} &= \lambda_{k\rightarrow j} + \sigma_{k\rightarrow j}\phi \end{aligned} \tag{2}$$

where λ_j and σ_j are the decay constant and energy averaged absorption cross section of nuclide j respectively, $\lambda_{k\rightarrow j}$ and $\sigma_{k\rightarrow j}$ are the decay constant and the average cross section of nuclide *k* which leads to *j* respectively. And ϕ is the 1-group neutron flux.

As mentioned earlier, in fuel cycle calculations, the irradiation time is divided into sub-steps. At each time step, the transport, depletion and TH problems are solved separately and the solutions are iteratively coupled in a designated subroutine. The coupling scheme determines the accuracy and numerical stability of the solution.

Section 3.1 describes the beginning-of-step explicit method used in many of the existing computational tools used in reactor physics analyses. This is then followed by the SIE and SIMP algorithms introduction in Section 3.2 and 3.3 respectively. Lastly, the proposed SUB-STEP algorithm is presented in Section 3.4. The different numerical schemes presented in these sections describe the coupling procedure to solve the coupled problem for a single time-step with time step length $\Delta t = t_1 - t_0$. In addition, $\mathbf{N}_i$, $\mathbf{T}_i$ and $\boldsymbol{\mathcal{M}}_i$ are the nuclide density vector, TH conditions and transmutation matrix at t_i respectively.

3.1 Explicit Euler method

The most commonly used coupling approach is the beginning-of-step (BOS) method that is based on the explicit Euler method. Thermal-hydraulic (TH) iterations (index-*k*) for a pre-determined fuel inventory are performed at the BOS until reaction rate convergence is achieved. Then, the space and energy dependent microscopic reaction rates are assumed to be constant during the depletion time step. Knowing these reaction rates allows obtaining the concentration at the end-of-step (EOS) in a single calculation step.

1 $\boldsymbol{for}\ \kappa = 1{:}\,\kappa_{max}$

2 $\quad \boldsymbol{\mathcal{M}_0} \leftarrow \varphi(\mathbf{N}_0, \overline{\mathbf{T}}_0)$

3 $\quad \mathbf{T}_0^{(\kappa)} \leftarrow \Upsilon(\boldsymbol{\mathcal{M}_0})$

4 $\quad \overline{\mathbf{T}}_0 = \sum_{i=1}^{\kappa} \frac{\mathbf{T}_0^{(i)}}{\kappa}$

5 $\boldsymbol{end\ for}$

6 $\mathbf{N}_1 \leftarrow e^{\boldsymbol{\mathcal{M}}_0 \Delta t}\mathbf{N}_0$

In this work, different methods were compared with respect to their accuracy for a given number of iterations. Therefore, k_{max} in the above flowchart is fixed. An

alternative approach would be to provide a convergence criterion (or accuracy) and then compare the number of iterations required to achieve it.

The Explicit Euler method was shown to be prone to numerical stability issues (Kotlyar and Shwageraus, 2014). Furthermore, it uses the BOS reaction rates, which are assumed to be constant throughout the depletion step, thus leading to under- or over- prediction of the nuclide densities.

3.2 Stochastic Implicit Euler (SIE) method

SIE (Dufek et al., 2013b) is a recently proposed method that is not susceptible to numerical oscillations. In contrast to the BOS explicit method, in this method, the depletion and TH problems are solved simultaneously and iteratively with the transport problem. The solution is obtained by using the so-called stochastic approximation with under-relaxation factor based on the Robbins-Monro algorithm (1951). The relaxation algorithm could be either applied to the nuclide density field (i.e. SIE/ND) or the reaction rate field (i.e. SIE/FLUX). The mathematical derivation of the methods and their implementation is presented in the original paper and hence will not be repeated here.

Since the coupled MC calculations are computationally expensive, only the performance of the SIE/ND method is evaluated. Therefore, the SIE/ND algorithm will be referred to as just SIE throughout this paper.

In this method, the depletion calculations are performed with EOS flux and cross sections ($\boldsymbol{\mathcal{M}}_1$) rather than BOS quantities.

1 $\boldsymbol{\mathcal{M}_0} \leftarrow \varphi(\mathbf{N}_0, \mathbf{T}_0)$

2 $\overline{\mathbf{N}}_1 \leftarrow e^{\boldsymbol{\mathcal{M}}_0 \Delta t}\mathbf{N}_0$

$\overline{\mathbf{T}}_1 \leftarrow \Upsilon(\boldsymbol{\mathcal{M}_0})$

3 $\boldsymbol{for}\ \kappa = 1{:}\ \kappa_{max}$

4 $\boldsymbol{\mathcal{M}}_{\mathbf{1}}^{(\kappa)} \leftarrow \varphi(\overline{\mathbf{N}}_1, \overline{\mathbf{T}}_1)$

5 $\mathbf{N}_1^{(\kappa)} \leftarrow e^{\boldsymbol{\mathcal{M}}_{\mathbf{1}}^{(\kappa)}\Delta t}\mathbf{N}_0$

$\mathbf{T}_1^{(\kappa)} \leftarrow \Upsilon\left(\boldsymbol{\mathcal{M}}_{\mathbf{1}}^{(\kappa)}\right)$

6 $\overline{\mathbf{N}}_1 = \sum_{i=1}^{\kappa} \frac{\mathbf{N}_1^{(i)}}{\kappa} \quad \overline{\mathbf{T}}_1 = \sum_{i=1}^{\kappa} \frac{\mathbf{T}_1^{(i)}}{\kappa}$

7 $\boldsymbol{end\ for}$

3.3 Stochastic Implicit Mid-Point (SIMP) method

SIMP (Kotlyar and Shwageraus, 2014) is another recent method that uses a philosophy similar to that adopted in the SIE. However, the convergence procedure is performed with the middle-of-step (MOS) or time step-averaged quantities rather than the EOS ones. The relaxation algorithm could be applied either to the nuclide density field (i.e. SIMP/ND) or to the flux field (i.e. SIMP/FLUX). The mathematical derivation is presented in the original paper and hence will not be repeated. Only the performance of the SIMP/ND (denoted as SIMP) method will be reported. The results for the SIMP/FLUX method are expected to be similar.

In this method, the depletion calculations are performed with MOS (i.e. at $t_{0.5} = \frac{t_1+t_0}{2}$) reaction rates ($\boldsymbol{\mathcal{M}}_{0.5}$) and time step average TH properties ($\overline{\mathbf{T}}_{0.5}$).

$\boldsymbol{\mathcal{M}}_{\mathbf{0}} \leftarrow \varphi(\mathbf{N}_0, \mathbf{T}_0)$

$\overline{\mathbf{N}}_1 \leftarrow e^{\boldsymbol{\mathcal{M}}_0 \Delta t}\mathbf{N}_0$

$\overline{\mathbf{T}}_{0.5} \leftarrow \Upsilon(\boldsymbol{\mathcal{M}}_{\mathbf{0}})$

for $\kappa = 1 : \kappa_{max}$

$$\boldsymbol{\mathcal{M}}_{\mathbf{0.5}}^{(\kappa)} \leftarrow \varphi\left(\frac{\overline{\mathbf{N}}_1 + \mathbf{N}_0}{2}, \overline{\mathbf{T}}_{0.5}^{(\kappa-1)}\right)$$

$$\mathbf{N}_1^{(\kappa)} \leftarrow e^{\boldsymbol{\mathcal{M}}_{\mathbf{0.5}}^{(\kappa)} \Delta t}\mathbf{N}_0$$

$$\mathbf{T}_{0.5}^{(\kappa)} \leftarrow \Upsilon\left(\boldsymbol{\mathcal{M}}_{\mathbf{0.5}}^{(\kappa)}\right)$$

$$\overline{\mathbf{N}}_1 = \sum_{i=1}^{\kappa} \frac{\mathbf{N}_1^{(i)}}{\kappa} \qquad \overline{\mathbf{T}}_{0.5} = \sum_{i=1}^{\kappa} \frac{\mathbf{T}_{0.5}^{(i)}}{\kappa}$$

end for

3.4 Sub-step method

The methods presented in Sections 3.1, 3.2 and 3.3 are limited to a constant power/flux approximation, in which either the BOS, EOS or MOS reaction rates are considered to be representative of the entire time step. The stochastic semi-implicit sub-step (denoted as SUBSTEP) method presented here is an extension to a recently suggested revised sub-step methodology for coupled MC depletion analysis (Kotlyar and Shwageraus, 2016). In this approach, the main idea was to create a relation between the reaction rates and the logarithm of nuclide densities and then apply the sub-step method to account for the reaction rates change as a function of nuclide densities. This method was inspired by the sub-step scheme originally introduced by Isotalo and Aarnio (2014) and the improved log-linear rate method (Carpenter et al., 2010) that has been developed for MC21 Monte Carlo code (Sutton et al., 2007).

The main idea of the proposed method is to create a relation between the reaction rates and the nuclide densities as well as the TH conditions (stage 5 in the flow chart presented below). A functional relationship needs to be assumed between the reaction rates, thermal-hydraulic conditions and nuclide densities. The choice of this relation will be discussed in subsequent section. The correlation coefficients can then be updated as more data becomes available with each additional iteration. The sub-step approach was incorporated into the SIE method. In this approach, the time step is divided into sub-steps and the depletion and TH problems are solved separately for each sub-step (stages 7 through 12 in the below chart). This sub-step method accounts for the change in reaction rates without requiring additional MC solutions. First, the reaction rates are updated (Stage 10 in the flow chart) due to the variation of nuclide densities (Stage 9). These reaction rates are then used to calculate the new TH conditions (Stage 11), which in turn change the reaction rates for the subsequent sub-step (Stage 8).

1 $\boldsymbol{\mathcal{M}_0} \leftarrow \varphi(\mathbf{N}_0, \mathbf{T}_0)$

2 $\overline{\mathbf{N}}_1 \leftarrow e^{\boldsymbol{\mathcal{M}}_0 \Delta t}\mathbf{N}_0$

$\overline{\mathbf{T}}_1 = \mathbf{T}_0 \leftarrow \Upsilon(\boldsymbol{\mathcal{M}_0}, \mathbf{N}_0)$

3 $\boldsymbol{for}\ \kappa = 1{:}\,\kappa_{max}$

4 $\boldsymbol{\mathcal{M}_1} \leftarrow \varphi(\overline{\mathbf{N}}_1, \overline{\mathbf{T}}_1)$

5 $\boldsymbol{\mathcal{M}_t} \equiv \boldsymbol{\mathcal{M}_t}(\mathbf{N}_t, \mathbf{T}_t)$

6 $\mathbf{N}_\ell^{(\kappa)} = \mathbf{N}_0 \quad \mathbf{T}_\ell^{(\kappa)} = \mathbf{T}_0$

7 $\boldsymbol{for}\ \ell = 1{:}\,\ell_{max}$

8 $\boldsymbol{\mathcal{M}_\ell} \leftarrow \boldsymbol{\mathcal{M}_t}\left(\mathbf{N}_\ell^{(\kappa)}, \mathbf{T}_\ell^{(\kappa)}\right)$

9 $\mathbf{N}_{\ell+1}^{(\kappa)} \leftarrow e^{\boldsymbol{\mathcal{M}}_\ell \times \frac{\Delta t}{\ell_{max}}}\mathbf{N}_\ell^{(\kappa)}$

10 $\boldsymbol{\mathcal{M}_\ell} \leftarrow \boldsymbol{\mathcal{M}_t}\left(\mathbf{N}_{\ell+1}^{(\kappa)}, \mathbf{T}_\ell^{(\kappa)}\right)$

11 $\mathbf{T}_{\ell+1}^{(\kappa)} \leftarrow \Upsilon\left(\boldsymbol{\mathcal{M}}_\ell, \mathbf{N}_{\ell+1}^{(\kappa)}\right)$

12 $\boldsymbol{end\ for}{:}\ \ell$

13 $\overline{\mathbf{N}}_1 = \sum_{i=1}^{\kappa} \frac{\mathbf{N}_1^{(i)}}{\kappa} \quad \overline{\mathbf{T}}_1 = \sum_{i=1}^{\kappa} \frac{\mathbf{T}_1^{(i)}}{\kappa}$

14 $\boldsymbol{end\ for}{:}\ \kappa$

The variables $\mathbf{N}_t$ and $\boldsymbol{\mathcal{M}}_t$ in stage 5 are nuclide densities and reaction rates as a function of time respectively. These variables are constructed from knowing the BOS $\mathbf{N}_0$ and $\boldsymbol{\mathcal{M}}_0$ and EOS $\mathbf{N}_1$ and $\boldsymbol{\mathcal{M}}_1$ values. It must be pointed out that the same correlation (described in section 3.4.3) to obtain $\boldsymbol{\mathcal{M}}_t$ will be used in all subsequent sub-steps. However, the correlation coefficients will be updated with each subsequent iteration as we obtain more MC transport solutions.

The method presented here is a general one and can be used in coupled problems where depletion and TH feedbacks are important. However, the method can also be used for problems with no TH feedback, such as cases with reduced dimensionality. The iterations can be switched off by setting κ_{max} to 1.

3.4.1 Derivation of the sub-step scheme within the time step

This section describes how the link between the reaction rates and other parameters of interest is established. The first stage includes generation of data at BOS and EOS time points, from which the reaction rates are tabulated as a function of nuclide densities and temperatures. These data points are stored for each nuclide and reaction type. According to the SIE methodology, depletion and TH calculations are performed simultaneously. Therefore, the input variables (i.e. nuclide densities and thermal hydraulic conditions) are passed to the transport solver to obtain the corresponding reaction rates, as schematically illustrated in Fig. 1.

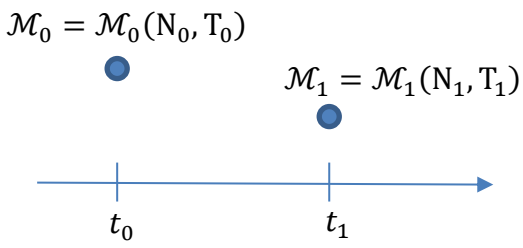

Fig. 1. Schematic illustration of the change in reaction rates $(\mathcal{M})$ as a function of nuclide densities (N) and temperatures (T)

The main assumption that we make here is that the reaction rates in $[t_0, t_1]$ may be obtained through interpolation in the following manner:

$$\mathcal{M}(\mathrm{N}, \mathrm{T}) = [1 - \theta(\mathrm{N}, \mathrm{T})]\mathcal{M}_0 + \theta(\mathrm{N}, \mathrm{T})\mathcal{M}_1 \quad (3)$$

where the weighting parameter $\theta \in [0,1]$ depends on the nuclide density and TH conditions. For simplicity, we will assume here that TH conditions are represented by the fuel temperature only. However, the described methodology can be easily extended to a more generic case, where TH conditions could also include coolant temperature, density, etc.

We now assume that if the nuclide densities are fixed and only the temperature varies, then, assuming linear reaction rate dependence on temperatures we obtain:

$$\theta(\mathrm{N}, \mathrm{T}) = \theta(\mathrm{T}) = \frac{\mathrm{T} - \mathrm{T}_0}{\mathrm{T}_1 - \mathrm{T}_0} \quad (4)$$

Or, alternatively, if the temperatures are fixed and only the nuclide densities are changed then, assuming the reaction rates vary linearly with the logarithm of nuclide densities, we obtain:

$$\theta(\mathrm{N},\mathrm{T}) = \theta(\mathrm{N}) = \frac{ln\frac{\mathrm{N}}{\mathrm{N_0}}}{ln\frac{\mathrm{N_1}}{\mathrm{N_0}}} \tag{5}$$

More detailed reasoning behind the correlations presented in Eqs. 4 and 5 will be explained in Section 3.4.3.

In reality however, both nuclide densities and temperatures are varied simultaneously and therefore both changes should be accounted for. This may be achieved by assigning weighting/importance factors as described in Eq. 6 below.

$$\theta(\mathrm{N},\mathrm{T}) = w(\mathrm{N},\mathrm{T})\theta(\mathrm{N}) + [1 - w(\mathrm{N},\mathrm{T})]\theta(\mathrm{T}) \tag{6}$$

The $w(\mathrm{N},\mathrm{T})$ weight can be approximated by the following relation:

$$w(\mathrm{N},\mathrm{T}) = \frac{\left|\frac{\partial\mathcal{M}}{\partial\mathrm{N}}\right| |\mathrm{N} - \mathrm{N_0}|}{\left|\frac{\partial\mathcal{M}}{\partial\mathrm{N}}\right| |\mathrm{N} - \mathrm{N_0}| + \left|\frac{\partial\mathcal{M}}{\partial\mathrm{T}}\right| |\mathrm{T} - \mathrm{T_0}|} \tag{7}$$

The numerator in Eq. 7 describes the absolute change in reaction rates due to the change in nuclide densities. Therefore, the weight coefficient, $w(\mathrm{N},\mathrm{T})$, describes the importance of change in nuclide densities relative to the total change in both nuclide densities and TH conditions.

The derivatives $\frac{\partial\mathcal{M}}{\partial\mathrm{N}}$ and $\frac{\partial\mathcal{M}}{\partial\mathrm{T}}$ in Eq. 7 can be approximated by applying a standard perturbation theory as follows. For the changes $\Delta\mathrm{N}$ and $\Delta\mathrm{T}$, the reaction rates $\mathcal{M}$ at a perturbed state can be expressed using a Taylor series expansion:

$$\mathcal{M}(\mathrm{N_0} + \Delta\mathrm{N}, \mathrm{T_0} + \Delta\mathrm{T}) = \mathcal{M}_0 + \frac{\partial\mathcal{M}}{\partial\mathrm{N}}\Delta\mathrm{N} + \frac{\partial\mathcal{M}}{\partial\mathrm{T}}\Delta\mathrm{T} + \mathrm{O}[(\Delta\mathrm{N})^2, (\Delta\mathrm{T})^2] \tag{8}$$

In order to obtain the derivatives $\frac{\partial\mathcal{M}}{\partial\mathrm{N}}$ and $\frac{\partial\mathcal{M}}{\partial\mathrm{T}}$, we need to solve the following system of equations

$$\begin{bmatrix} \Delta \mathrm{N}^{(i-1)} & \Delta \mathrm{T}^{(i-1)} \\ \Delta \mathrm{N}^{(i)} & \Delta \mathrm{T}^{(i)} \end{bmatrix} \begin{bmatrix} \frac{\partial \mathcal{M}}{\partial \mathrm{N}} \\ \frac{\partial \mathcal{M}}{\partial \mathrm{T}} \end{bmatrix} = \begin{bmatrix} \mathcal{M}^{(i-1)} - \mathcal{M}_0 \\ \mathcal{M}^{(i)} - \mathcal{M}_0 \end{bmatrix} \tag{9}$$

where

$$\begin{aligned} \Delta \mathrm{N}^{(i)} &= \mathrm{N}_1^{(i)} - \mathrm{N}_0 \\ \Delta \mathrm{T}^{(i)} &= \mathrm{T}_1^{(i)} - \mathrm{T}_0 \end{aligned} \tag{10}$$

And the superscript i denotes the iteration index. According to this approach, the derivatives are iteration's dependent and the procedure for calculating the derivatives can only start for $i > 1$.

3.4.2 Sub-step procedure

This section describes the practical implementation of the sub-step methodology within the time step $t \in [t_0, t_1]$. Let us assume that the time step is divided into 10 equal length sub-steps. Then, the following procedure is applied:

1. For fixed N_0 and T_0, the reaction rates, $\mathcal{M}_0$, are evaluated from the neutron transport solution (MCNP) at t_0.
2. The reaction rates $\mathcal{M}_0$ are simultaneously used in depletion and TH calculations with a time step of $t_1 - t_0$.
3. As a result, the EOS N_1 and T_1 are obtained and used in the transport calculations to obtain the EOS reaction rates $\mathcal{M}_1$.
4. The sub-step procedure restarts at t_0, where N_0, T_0 and $\mathcal{M}_0$ (stage 1) are known.
5. Assuming that the reaction rates $\mathcal{M}_0$ are constant within the first sub-step $(t_1 - t_0)/10$, the nuclide densities N_t are obtained.
6. Equations 3-10 are used to obtain the updated $\mathcal{M}_t$.
7. These updated reaction rates $\mathcal{M}_t$ are used to recalculate the power distribution.
8. The updated power distribution is used to update the temperatures T_t.
9. The temperatures T_t are used in eqs. 3-10 to obtain the updated $\mathcal{M}_t$.
10. At this point, N_t, T_t and $\mathcal{M}_t$ are known at $(t_1 - t_0)/10$ and stages 4-9 are repeated for all subsequent sub-steps within the time step by varying N_t, T_t and $\mathcal{M}_t$.

3.4.3 Reaction rates correlations

PWR unit cell with UO_2 (3.5 w/o of U^{235}) is used here to demonstrate the impact of different input parameters (e.g. nuclide densities and TH conditions) on various microscopic reaction rates (i.e. microscopic cross section multiplied by the flux). Fig. 2 shows a schematic view of the unit cell. The UO_2 fuel is mixed with 1.5 v/o of Gd_2O_3 and has a radius of 0.4095 cm. The thickness of the Zirconium clad is 0.0655 cm and the fuel pin pitch is 1.26 cm. The boundary conditions in all directions are reflective.

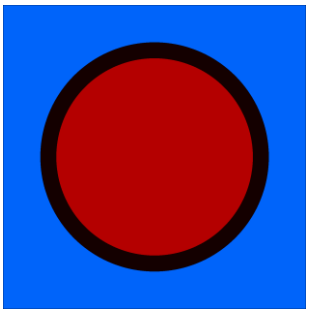

Fig. 2. PWR unit cell

Fig. 3 and Fig. 4 illustrate the reasoning behind the correlation used in Eqs. 4-5.
For this purpose, the reaction rates were plotted for each of the separate input variables, i.e. nuclide concentration - N (Fig. 3) and fuel temperature - T_f (Fig. 4). No burnup calculations were carried out here, but rather static MC calculations, in which each of the input parameters was varied and the corresponding reaction rates ($\mathcal{M}$) are obtained and presented in the figures. It should be noted that the fuel composition also included fission products, plutonium, and minor actinides obtained by depleting the UO_2 fuel in
advance. For each of the input variables, a least square fit curve is also shown. As can be seen from these figures, different correlations were chosen to best represent the dependence of the reaction rates on nuclide densities and TH conditions. The correlations are summarized in Eq. 11 and justify the assumptions used in Eqs. 4-5.

$$\mathcal{M}(N) = A_1 \ln N + A_2$$
$$\mathcal{M}(T_f) = A_3 T_f + A_4 \quad (11)$$

It must be pointed out that higher order correlations could also be suitable. However, such analysis was outside the scope of the current study but it is planned to be covered in future research.

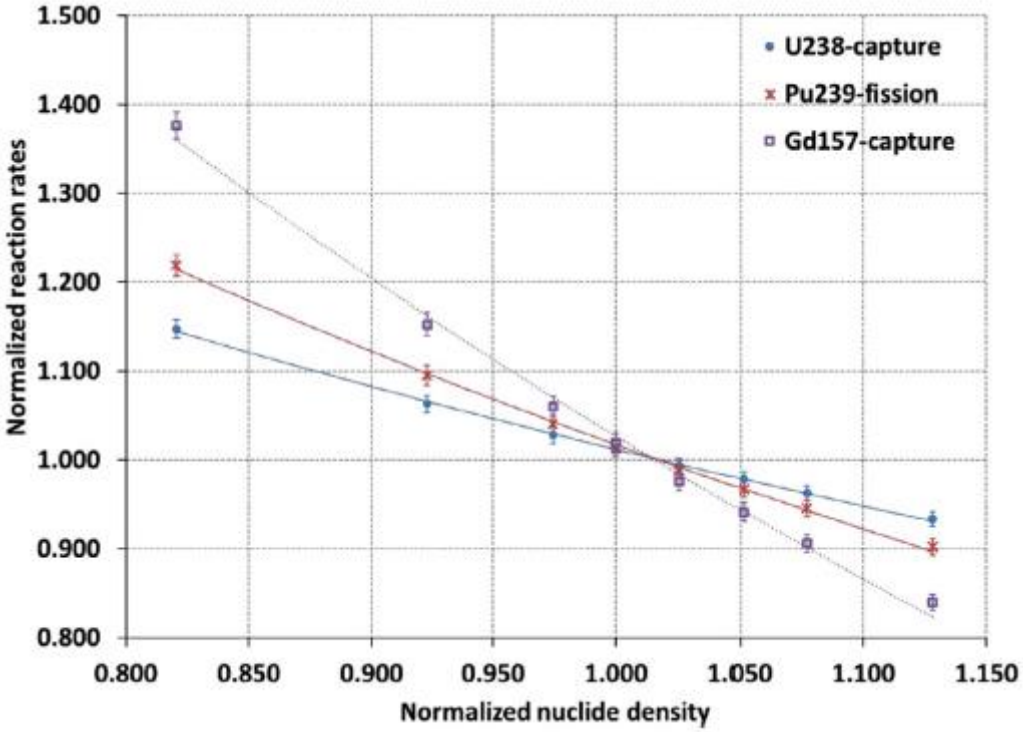

Fig. 3. Reactions rates as a function of concentration

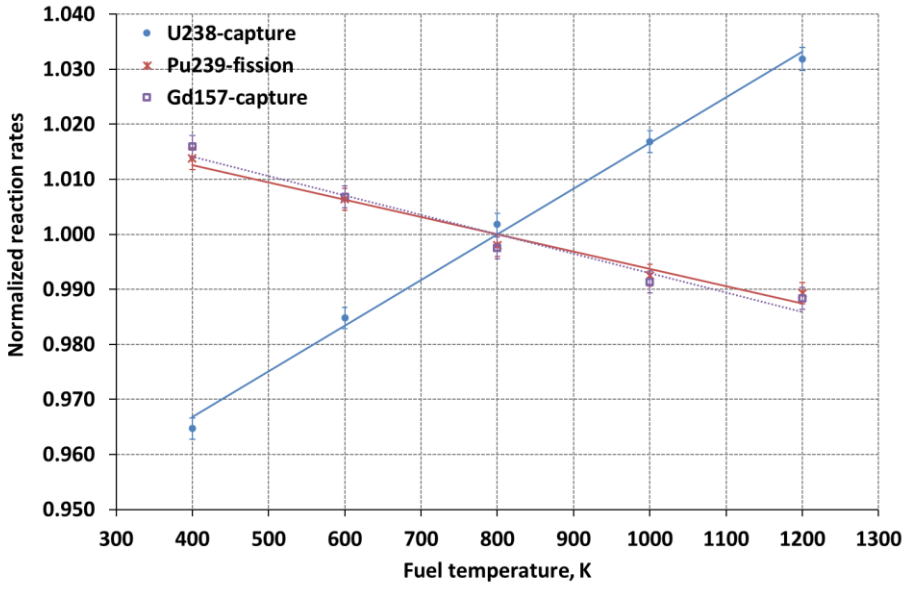

Fig. 4. Reactions rates as a function of fuel temperature

4. Results and discussion

Two 3D test cases were analyzed to demonstrate the proposed method. For both cases, a reference solution was generated by the SIE method with ultra-fine time steps. Section 4.1 presents the results for a typical PWR 3D unit cell for which all the analyzed methods produce relatively accurate results. Section 4.2 presents a somewhat more realistic 3D case, in which Gd_2O_3 is used as a burnable absorber and due to which, the flux amplitude and spectrum change rapidly with time. This section shows, that neither of the previously proposed methods (i.e. explicit, SIE and SIMP) could accurately capture the real behavior, while adopting the new sub-step method has shown to be successful in achieving that.

4.1 PWR 3D unit cell

PWR unit cell with UO_2 (3.5 w/o of U^{235}) is used to show that for cases where the spectrum varies slowly with time, the SIE and SIMP methods produce relatively accurate results. Additional objective is to explore the sensitivity of accuracy of the results to the length of the time step. Therefore, the analyses were performed for typical values of 60 days and then repeated for 120 days' time steps. Typical PWR power density of 104 W/cm^3 which corresponds to 38 MW/kgHM was used.
The radial and axial schematic views of the examined case are shown in Fig. 5. The pin dimensions are identical to those reported in Table 1.

The active height of the fuel is 366 cm and was divided into 12 equal height axial layers which included identical materials at the beginning of irradiation campaign. The bottom (20 cm) and upper (20 cm) reflectors were modeled as homogeneous mixtures of water and stainless steel. The mass flow rate for this single TH channel was 0.3 kg/sec. Each neutron transport calculation with MCNP used 150 active fission source iteration cycles with 50,000 histories per cycle. Sensitivity studies varying the number of active cycles were performed. The results indicated that 150 active cycles are sufficient to assure the source convergence.

The different coupling approaches were compared to the reference solution. This solution was obtained using fine time steps of 10 days with SIE method. In all methods, a fixed number of 10 iterations was used.

The results are presented in Fig. 6 through Fig. 9. The results show that the SUBSTEP method outperforms the SIE, SIMP and the explicit methods. Moreover, the results indicate that when the time step is increased from 60 days to 120 days, the performance of the SIE and explicit methods is significantly deteriorated, while there is almost no impact on the accuracy of results when the SIMP and SUBSTEP methods are adopted.

Fig. 6 presents the difference in reactivity for various methods. When 60 days time steps are used (Fig. 6a), the results obtained with the SIE and SIMP generate relatively accurate results with maximum reactivity difference below 100 pcm. The prediction of reactivity with the explicit method is somewhat poorer with maximum reactivity difference slightly below 200 pcm. The results obtained with the SUBSTEP method are within the statistical uncertainties (1σ). Moreover, the explicit and SIE methods produce less accurate results when the time step is increased to 120 days (Fig. 6b), with a maximum difference of 340 and 200 pcm respectively. Fig. 7 and Fig. 8 show the relative difference in Pu^{239} and U^{235} concentration as a function of time. Again, the SUBSTEP produces more accurate results than the SIMP, SIE and the explicit methods. Lastly, Fig. 9 presents the axial Pu^{239} distribution at the end of the irradiation campaign (at 920 days). These figures show that the explicit method under-predicts and the SIE over-predicts the overall distribution. These differences are further increased when a larger time step is used. However, a good agreement in Pu^{239} distribution is observed when the sub-step or SIMP methods are used.

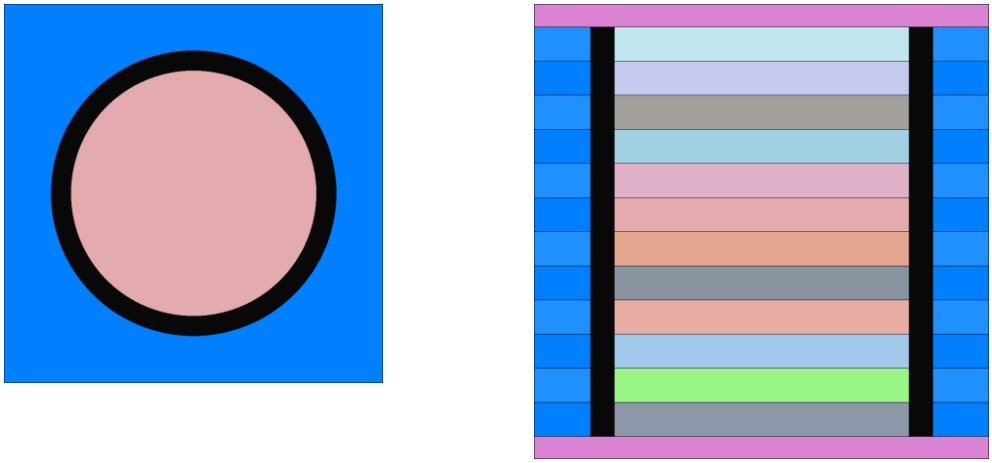

(a) x-y view (b) x-z view

Fig. 5. PWR 3D unit cell

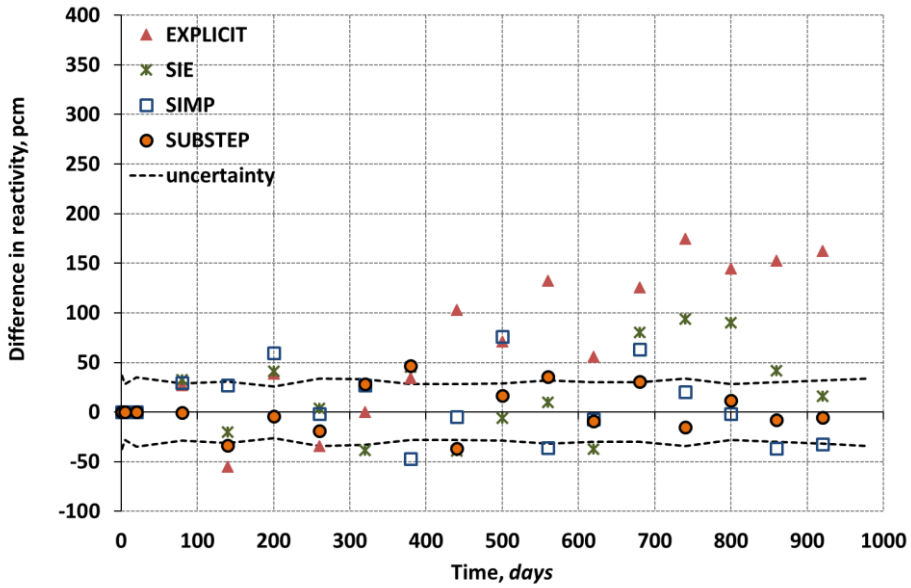

(a) 60 days time step

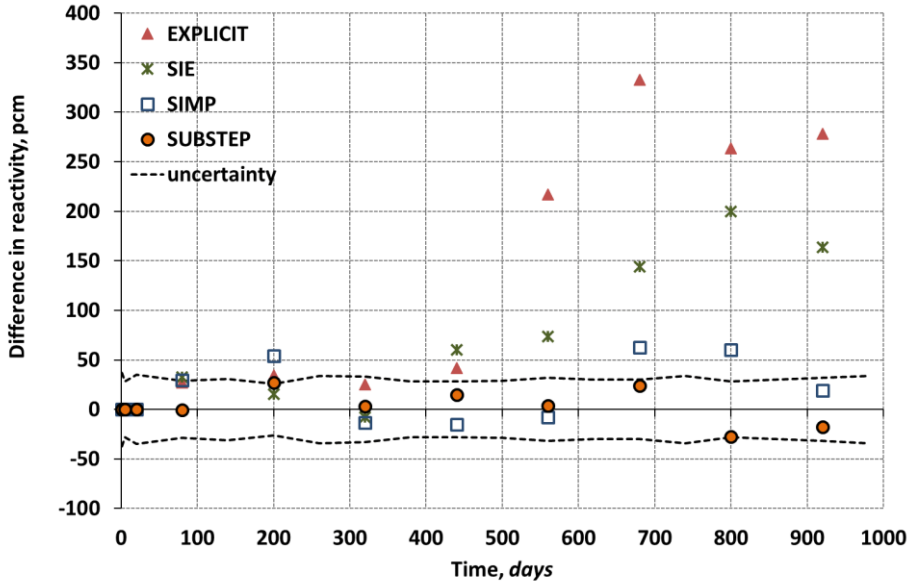

(b) 120 days time step

Fig. 6. Comparison of k-inf for various coupling schemes, unit cell case

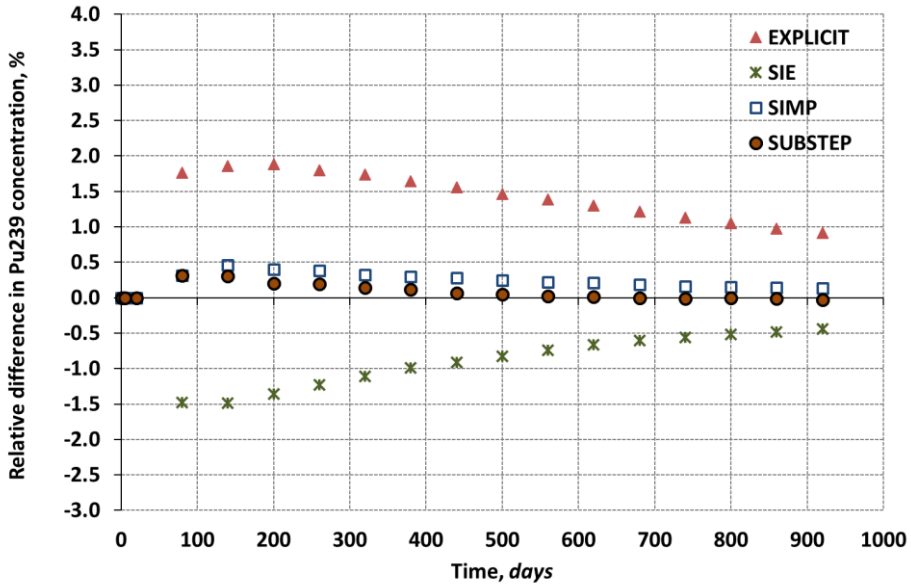

(a) 60 days time step

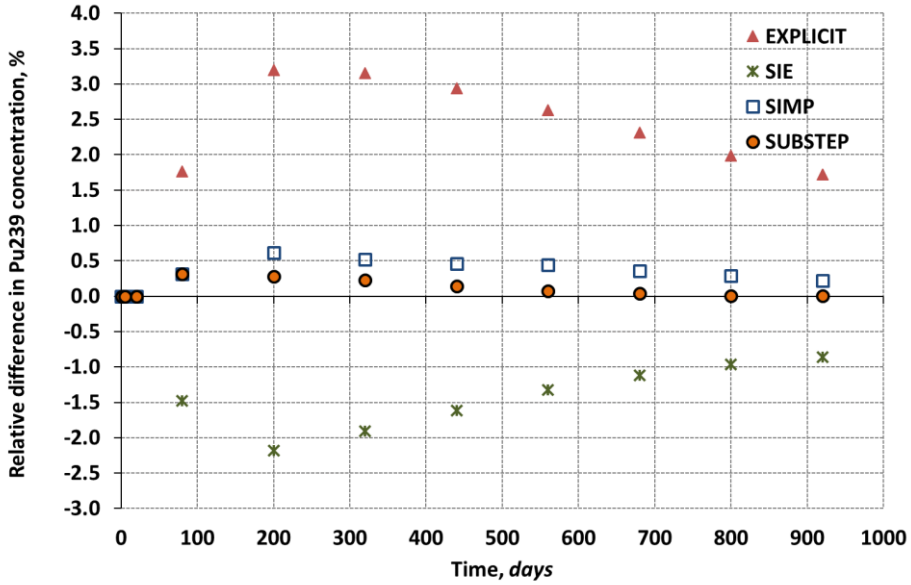

(b) 120 days time step

Fig. 7. Comparison of Pu^{239} concentration for various coupling schemes, unit cell case

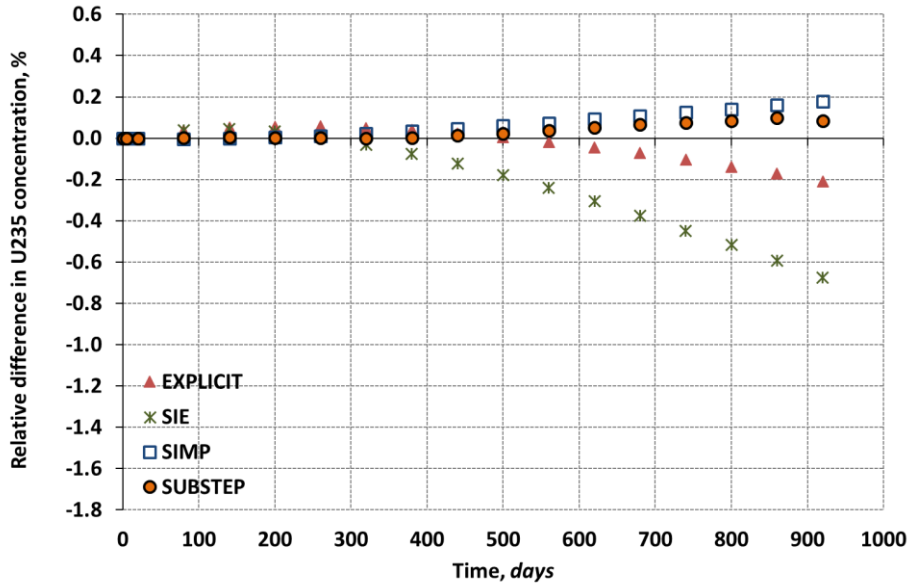

(a) 60 days time step

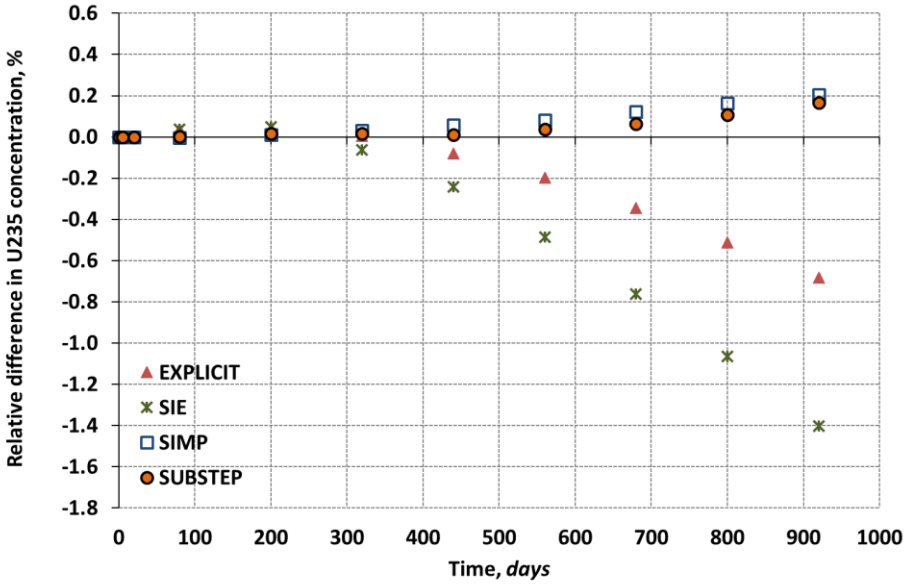

(b) 120 days time step

Fig. 8. Comparison of U^{235} concentration for various coupling schemes, unit cell case

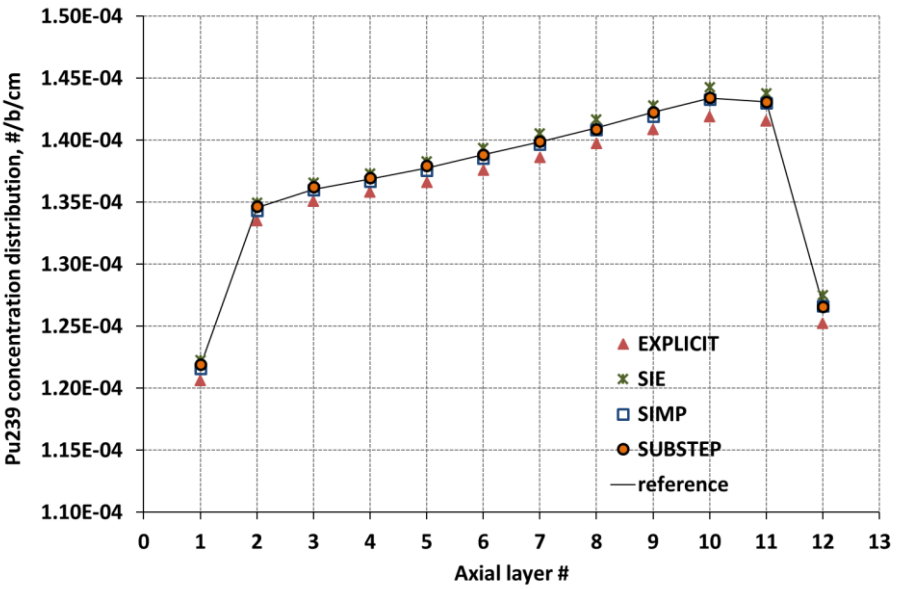

(a) 60 days time step

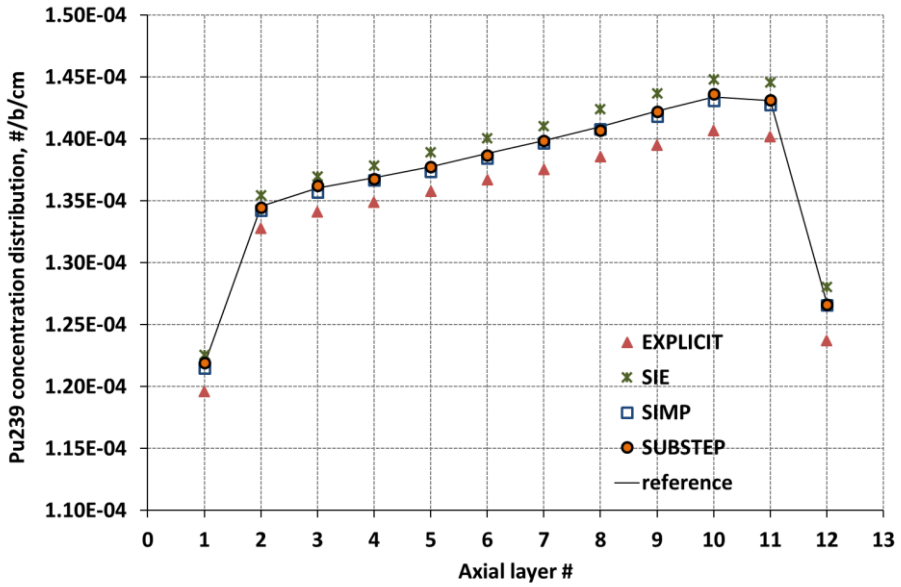

(b) 120 days time step

Fig. 9. Comparison of Pu^{239} axial distribution for various coupling schemes, unit cell case

4.2 PWR 3D mini-assembly with Gadolinium

A 3×3 array of PWR pins with UO_2 fuel (Kotlyar et al., 2015) is examined in this section. The initial fuel enrichment was taken to be 3.5 w/o. The fuel in the central pin was mixed with 1.5 v/o of Gd_2O_3. The central pin was radially subdivided into 5 equal-volume regions to realistically track the spatial burnup of Gd isotopes and its effect on the system's criticality. Axially, the active fuel was divided into 12 equal length axial layers, 30 cm each. Bottom and upper reflectors contained a homogeneous water-stainless steel mixture. Schematic view and operating parameters of the considered mini-assembly test case are given in Fig. 10 and Table 1.

In order to obtain relatively small statistical uncertainties, 250 active fission source iteration cycles with 100,000 histories per cycle were used in the neutron transport calculations with MCNP. The efficiency of each scheme to achieve a certain convergence was not studied here and rather a fixed number of 10 iterations was used in all cases.

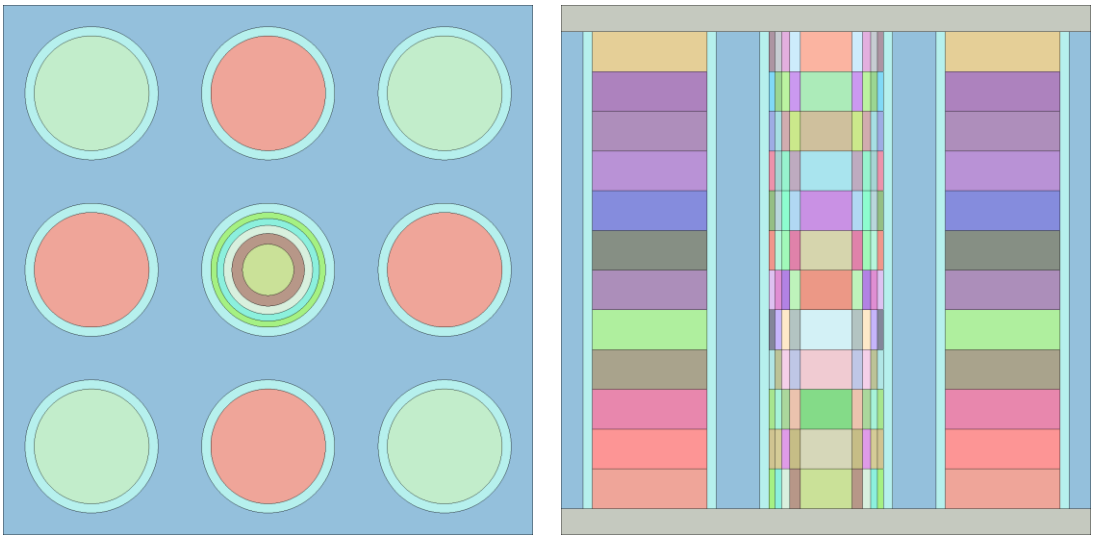

a. Radial layout b. Axial layout

Fig. 10. PWR mini-assembly geometry

Table 1: Summary of the mini-assembly design parameters

Parameter	**Value**
Fuel pellet diameter, cm	0.8100
Fuel pin diameter, cm	0.9500
Cladding thickness, cm	0.0655
Fuel lattice pitch, cm	1.2600
Number of pins per assembly	9
Active height, cm	360
Total height, cm	400
Power, W/cm^3	104
$\dot{m}$, kg/sec	19.20

The chosen problem includes Gd absorber which strongly affects the system's neutron energy spectrum and hence criticality. In the current study, only the time interval between 0 and 110 days associated with Gd depletion was analyzed to illustrate the issues related to the different coupling schemes.

The reference solution was obtained by using SIE method with very fine time steps of 0.25 days or 0.009 MWd/kg. The solutions with various methods were

obtained for 5 days time step and repeated for more practical time steps of 20 days. Fig. 11 presents the system criticality as a function of time obtained using different methods.

Fig. 12a depicts the difference in reactivity (pcm) between the reference and the four studied coupling schemes. The figure shows that there is an under-prediction and over-prediction in reactivity when either explicit or the SIE methods are used respectively. The figure also shows that considerable improvement is achieved when SIMP is used, but there is still a slight under-prediction of 250 pcm. Fig. 12b shows that increasing the time step amplifies the error, e.g. from 1500 pcm to >2000 pcm or from -250 to -1000 pcm when SIE or SIMP methods are used respectively. These discrepancies are practically diminished when the sub-step method is used. In general, the explicit, SIE and SIMP methods are not capable of capturing the realistic (i.e. close to reference) behavior of all neutronic and TH parameters as shown in Fig. 13 and Fig. 14. Fig. 13 presents the axial distribution of Gd^{157} in the central pin at 30 days time point. Fig. 14 shows the axial centerline fuel temperature distribution in the central pin. One can notice that the explicit method tends to over-predict the Gd^{157} concentration (Fig. 13) around the core mid-plane, which, in turn, leads to under-prediction of the power and fuel temperature (Fig. 14) due to the artificially increased absorption in that region. The behavior of the results when SIE method is adopted is the opposite. In other words, concentration of Gd^{157} in the central regions is under predicted and results in over-prediction of the power and fuel temperatures.

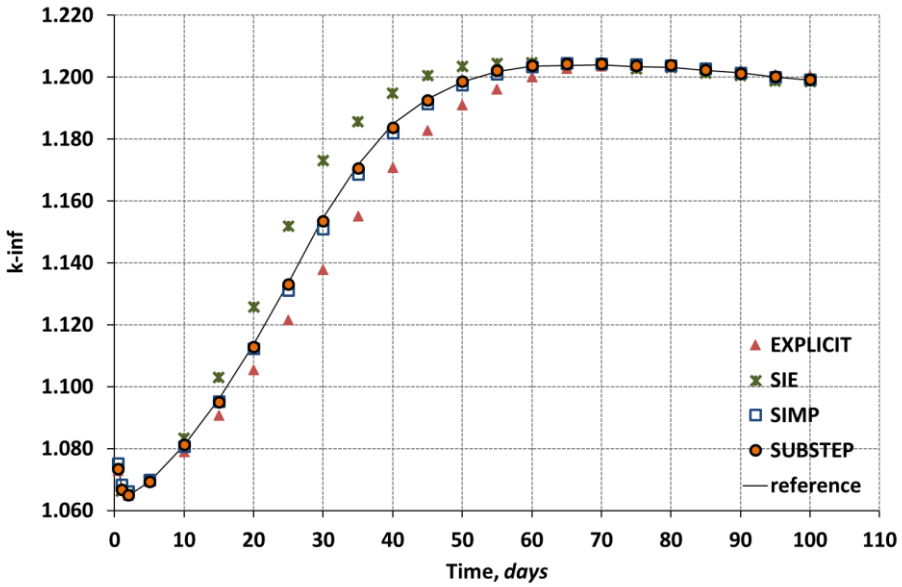

(a) 5 days time step

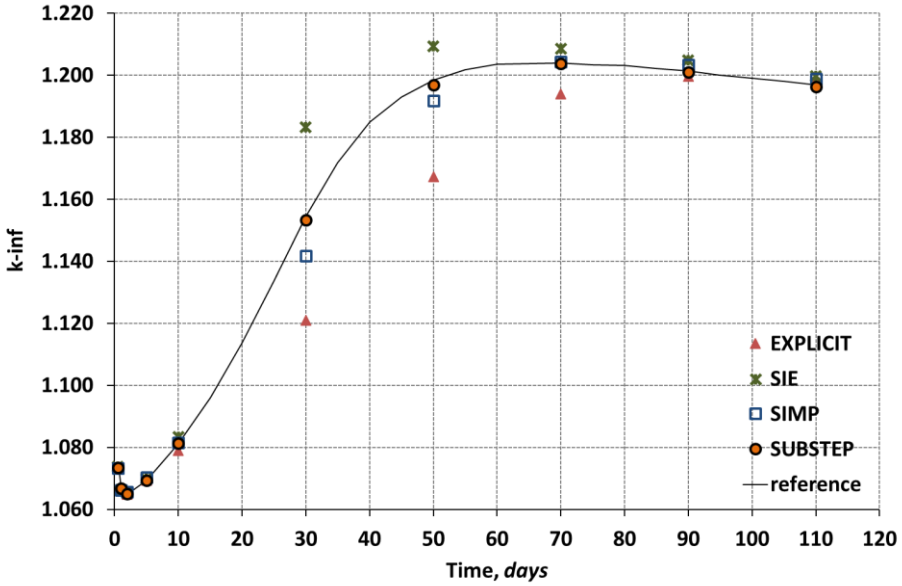

(b) 20 days time step

Fig. 11. k-inf for various coupling schemes, mini-assembly case

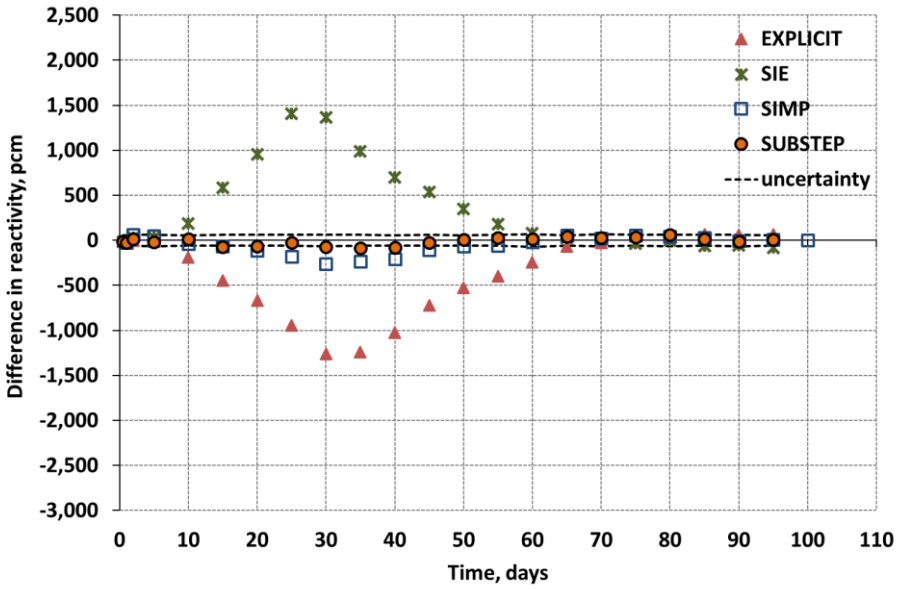

(c) 5 days time step

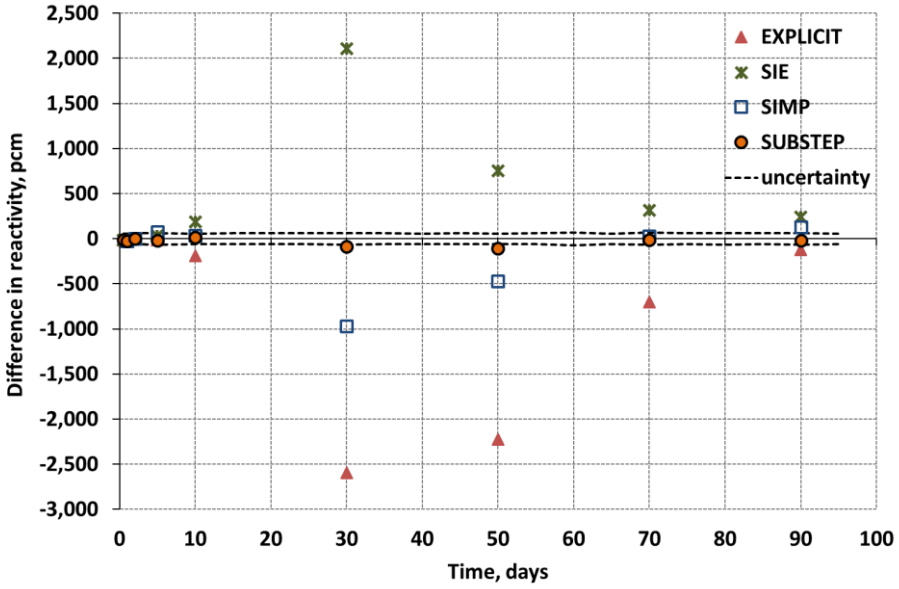

(d) 20 days time step

Fig. 12. Comparison of k-inf for various coupling schemes, mini-assembly case

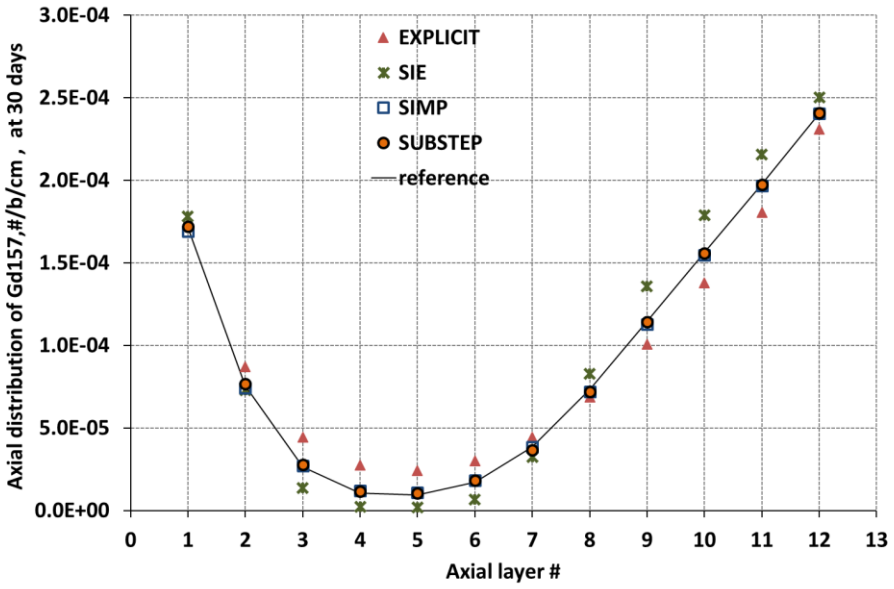

(a) 5 days time step

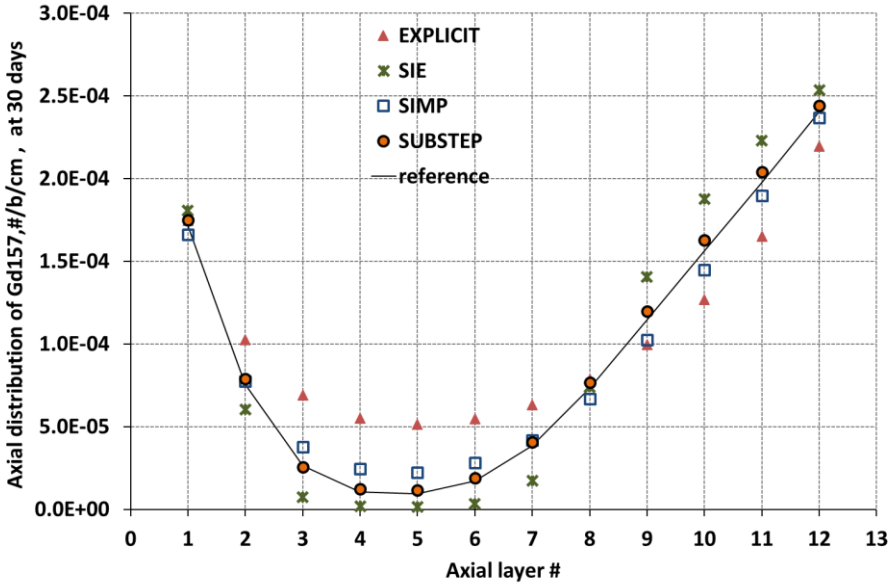

(b) 20 days time step

Fig. 13. Comparison of Gd^{157} axial distribution for various coupling schemes, mini-assembly case

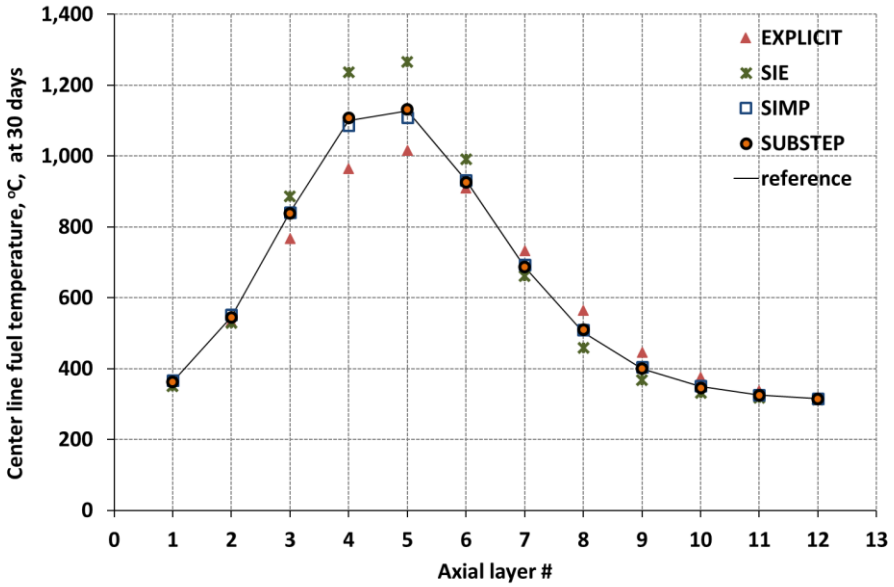

(a) 5 days time step

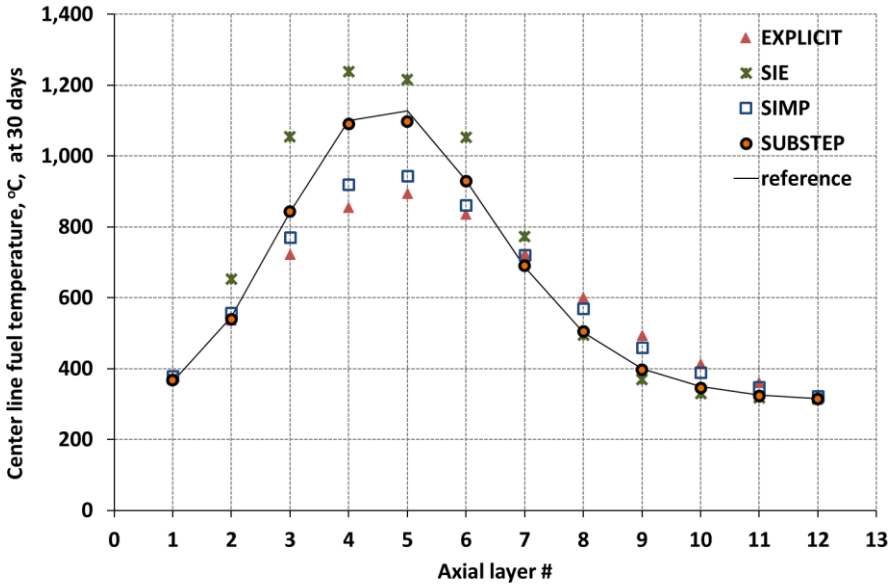

(b) 20 days time step

Fig. 14. Comparison of center line fuel temperature for various coupling schemes, mini-assembly case

Fig. 15 and Fig. 16 demonstrate the effectiveness of the sub-step method. For illustration purposes, only a single time interval of 20 days was examined. As mentioned earlier, the reference solution was obtained by depleting the problem with 0.25 days. Fig. 15 presents the reference total power of the central pin as a function of

time. This figure demonstrates that the power rapidly changes by ~25% within the examined 20 days time interval due to the rapid depletion of Gd^{157}. The reason that SIE and explicit methods perform poorly is the lack of information regarding the time-dependent reaction rates within the 20 days interval. The vertical lines in Fig. 15 show the explicit, SIE and SIMP powers used throughout the time step, which are assumed to be constant. The SUBSTEP extension allows to reproduce this time-dependent behavior and therefore achieves more accurate results. Fig. 16 demonstrates the axial power distribution for 3 sub-steps within the time step. It must be pointed out again that the reference solution was obtained by performing MC transport calculations every 0.25 days. The sub-step method on the other hand used the time steps of 20 days with sub-steps that required no additional MC solutions.

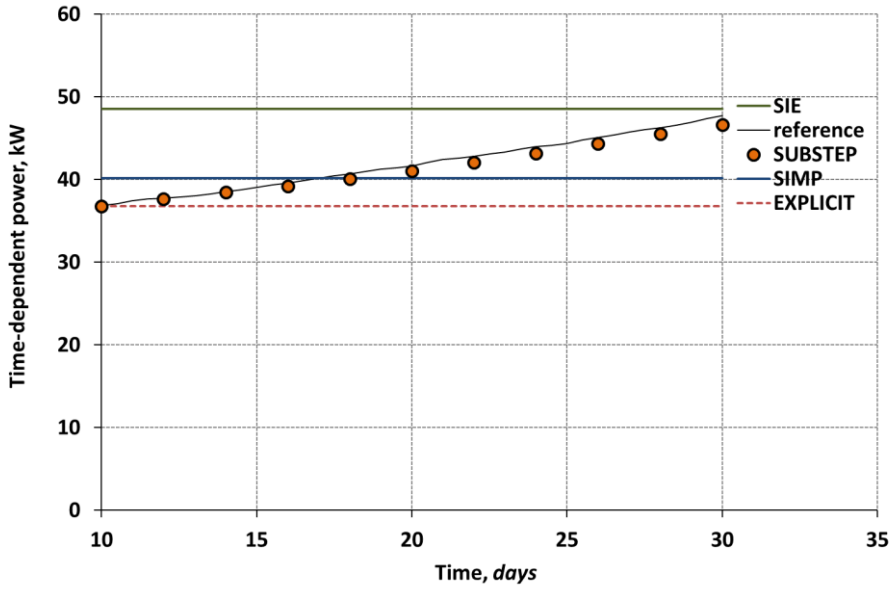

Fig. 15. Time-dependent power in the central pin for various coupling schemes, mini-assembly case.

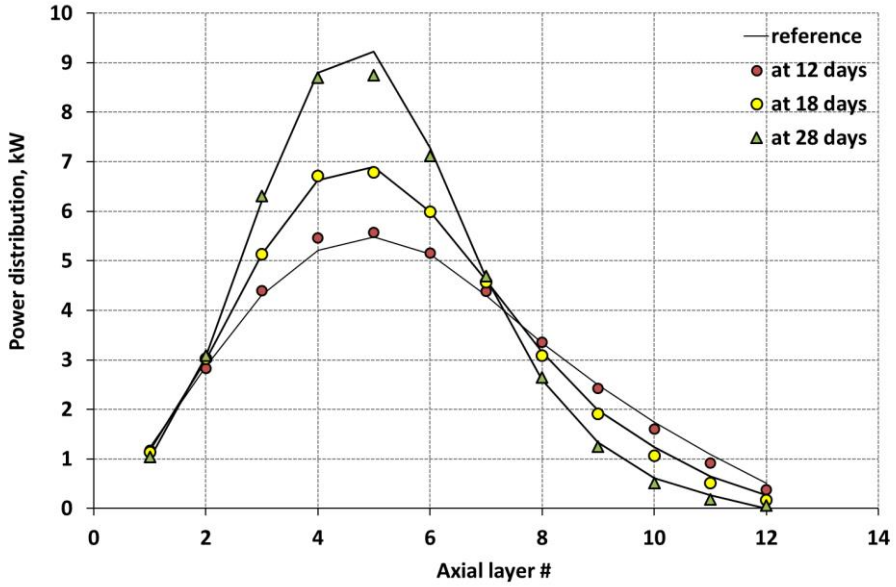

Fig. 16. Axial power distribution (central pin) for various coupling schemes, mini-assembly case.

5. Summary and Conclusions

Recent studies showed that traditional explicit coupling approaches can be numerically unstable. As a remedy to the stability issue, alternative methods (i.e. SIE and SIMP) were developed. In these methods, the depletion and thermal hydraulics feedbacks are solved simultaneously and iteratively with the transport problem. SIE method for example uses EOS fluxes to calculate EOS nuclide density and TH properties.

However, these methods rely on either constant EOS or MOS reaction rates throughout the entire time step. This assumption is valid only when the depletion steps are indeed sufficiently small and any spectrum variations are negligible. In reality, when practical time steps are used, the SIE and even SIMP are failing to produce accurate results. Moreover, if the stability issue could be ignored for the sake of an argument, explicit method would also fail to produce accurate results. The latter is a direct consequence of assuming constant BOS reaction rates values, which are certainly not representative of the entire time step.

The accuracy issues of the currently used and newly proposed methods was reported in recent studies (Kotlyar and Shwageraus, 2016). The problem identified

was associated with using discrete time point quantities rather than using the actual time dependent shape of the reaction rates. In previous studies, we proposed to extend the original SIE method by including the sub-step methodology. The method was verified on multiple 2D and 3D problems and demonstrated significantly better performance in terms of accuracy and hence computational efficiency. This was achieved by accounting for the reaction rates variation within the depletion time step without the need for additional MC transport solutions. However, the method was developed only for coupling the depletion feedback with the transport solution.

The current study focused on extending this methodology to incorporate simultaneous burnup-TH sub-step procedure also without requiring additional MC solutions. The method assumes that reaction rates are assumed functions of nuclide densities and fuel temperatures. The time step is divided into sub-steps, in which the depletion and TH calculations are performed. The updated nuclide densities and TH properties are then used to update the reaction rates. This routine is repeated for all subsequent sub-steps within the time step. This approach allows taking into consideration the variation of neutron spectrum due to the time-dependent variation of neutronic and TH properties.

Verification of the proposed method was performed on two 3D problems. The reference solution was obtained with ultra-fine time steps. In the examined cases, the SUBSTEP method demonstrated notably better performance in terms of accuracy and hence computational efficiency.

Future plans will focus on investigating higher order relations between the reaction rates and nuclide density and TH fields, which might improve the computational efficiency even further.

Acknolodgements

The authors would like to thank Ville Valtavirta from VTT for his help in reviewing this paper and providing insightful comments.

References

Bateman H., 1932. Partial Differential Equations of Mathematical Physics. Cambridge, University Press; New York, The Macmillan Co., 522+xii pp.

Bomboni E., Cerullo N., Fridman E., Lomonaco G., Shwageraus E., 2010. Comparison among MCNP-based depletion codes applied to burnup calculations of pebble-bed HTR lattices, Nuclear Engineering and Design, 240 (4), 918-924.

Briesmeister J. F. Ed., 2000. MCNP - A General Monte Carlo N-Particle Code, Version 4C, Los Alamos National Laboratory, LA-13709-M.

David C. Carpenter and Joseph H. Wolf III, 2010. The Log Linear Rate Constant Power Depletion Method, PHYSOR, Pittsburgh, Pennsylvania, USA, May 9-14.

Dufek J., Kotlyar D., Shwageraus E., Leppänen, J., 2013a. Numerical Stability of the Predictor-Corrector Method in Monte Carlo Burnup Calculations of Critical Reactors, Annals of Nuclear Energy, 56, 34-38.

Dufek J., Kotlyar D., Shwageraus E., 2013b. The Stochastic Implicit Euler Method - A Stable Coupling Scheme for Monte Carlo Burnup Calculations, Annals of Nuclear Energy, 60, 295-300.

Fensin M.L., Hendricks J.S., Trellue H.R., Anhaie S., 2006. The Enhancements and Testing for the MCNPX 2.6.0 Depletion Capability, Journal of Nuclear Technology, 170, 68-79.

Fridman E., Shwageraus E., Galperin A., 2008. Efficient generation of one-group cross sections for coupled Monte Carlo depletion calculations, Nuclear Science and Engineering, 159, 37-47.

Haeck W., Verboomen B., 2007. An optimum approach to Monte Carlo burnup, Nuclear Science and Engineering, 156, 180-196.

Isotalo A. and Aarnio P. A., 2011. Sub-step methods for burnup calculations with Bateman solutions, Annals of Nuclear Energy, 38, 2509, 2514.

Kotlyar D., Shaposhnik Y., Fridman E., Shwageraus E., 2011. Coupled neutronic thermo-hydarulic analysis of full PWR core with Monte-Carlo based BGCore system, Nuclear Engineering and Design, 241 (9), 3777-3786.

Kotlyar D., Shwageraus E., 2013. On the use of Predictor-Corrector Method for Coupled Monte Carlo Burnup Codes, Annals of Nuclear Energy, 58, 228-237.

Kotlyar D., Shwageraus E., 2014. Numerically stable Monte Carlo-Burnup-Thermal Hydraulic Coupling Schemes, Annals of Nuclear Energy, 63, 371-381.

Kotlyar D., Fridman E., Shwageraus E., 2015. One-group cross sections generation for Monte Carlo burnup codes: multi-group method extension and verification, Nuclear Science and Engineering, 179, 274-284.

Kotlyar D., Shwageraus E., 2016. Stochastic Semi-Implicit Sub-step Method for Coupled Depletion Monte-Carlo Codes, Annals of Nuclear Energy, 92, 52-60.

Leppänen, J., Mattila R., Pusa, M., 2014. Validation of the Serpent-ARES code sequence using the MIT BEAVRS benchmark - Initial core at HZP conditions. Annals of Nuclear Energy, 69, 212-225.

Leppänen, J., Pusa, M., Viitanen, T., Valtavirta, V. and Kaltiaisenaho, T., 2015. The Serpent Monte Carlo code: Status, development and applications in 2013. Annals of Nuclear Energy, 82, 142-150.

Robbins H. and Monro S., 1951. A Stochastic Approximation Method. Annals of Mathematical Statistics, 22, 400.

Sutton T. M., et al., 2007. The MC21 Monte Carlo Transport Code, Joint International Topical Meeting on Mathematics & Computation and Supercomputing in Nuclear Applications, M&C+SNA.